nature biomedical engineering

Article

https://doi.org/10.1038/s41551-024-01267-7

Optimization of the activity and biodegradability of ionizable lipids for mRNA delivery via directed chemical evolution

Received: 7 September 2023

Accepted: 21 September 2024

Published online: 22 November 2024

Check for updates

Xuexiang Han[1,2], Mohamad-Gabriel Alameh[3,4], Ying Xu[3], Rohan Palanki[1], Rakan El-Mayta[3], Garima Dwivedi[3], Kelsey L. Swingle[1], Junchao Xu[1], Ningqiang Gong[1], Lulu Xue[1], Qiangqiang Shi[1], Il-Chul Yoon[1], Claude C. Warzecha[5], James M. Wilson[5], Drew Weissman[3,4] & Michael J. Mitchell[1,4,6,7,8,9]

Ionizable lipids largely determine the biocompatibility of lipid nanoparticles (LNPs) and the efficacy for mRNA delivery. Rational design and combinatorial synthesis have led to the development of potent and biodegradable ionizable lipids, yet methodologies for the stepwise optimization of ionizable lipid structure are lacking. Here we show that iterative chemical derivatization and combinatorial chemistry, and in particular the amine–aldehyde–alkyne coupling reaction, can be leveraged to iteratively accelerate the structural optimization of propargylamine-based ionizable lipids (named A^3-lipids) to improve their delivery activity and biodegradability. Through five cycles of such directed chemical evolution, we identified dozens of biodegradable and asymmetric A^3-lipids with delivery activity comparable to or better than a benchmark ionizable lipid. We then derived structure–activity relationships for the headgroup, ester linkage and tail. Compared with standard ionizable lipids, the lead A^3-lipid improved the hepatic delivery of an mRNA-based genome editor and the intramuscular delivery of an mRNA vaccine against SARS-CoV-2. Structural criteria for ionizable lipids discovered via directed chemical evolution may accelerate the development of LNPs for mRNA delivery.

Messenger RNA (mRNA)-based therapeutics and vaccines are revolutionizing modern medicine approaches to treat or prevent diseases. The recent approval of three lipid nanoparticle (LNP)-based RNA drugs (Patisiran, mRNA-1273 and BNT162b2) and continuing advances in LNP technologies for mRNA therapeutics/vaccines and clustered regularly interspaced short palindromic repeats (CRISPR) gene editing have sparked great interest in this safe and effective non-viral vector[1,2]. The conventional LNP formulation comprises four components: ionizable lipids, phospholipids, cholesterol and polyethylene glycol (PEG)-conjugated lipids. An ionizable lipid typically consists of an amino headgroup and two (or more) alkyl tails that are connected by linkers, which plays a pivotal role in protecting and transporting RNA cargo[3,4]. Under acidic LNP formulation conditions, ionizable lipids are protonated and switched to a positively charged state, allowing for complexation with and encapsulation of anionic RNA molecules. At physiological pH, ionizable lipids remain neutral, thereby circumventing charge-related toxicity and improving the pharmacokinetic profile of LNPs. Following cellular uptake, the acidic environment of the endosome facilitates the protonation of ionizable lipids, leading to endosomal escape and release of mRNA[1].

Notably, ionizable lipids govern not only the potency but also the biocompatibility of LNPs. Therefore, current research focuses on

A full list of affiliations appears at the end of the paper. e-mail: mjmitch@seas.upenn.edu

https://doi.org/10.1038/s41551-024-01267-7

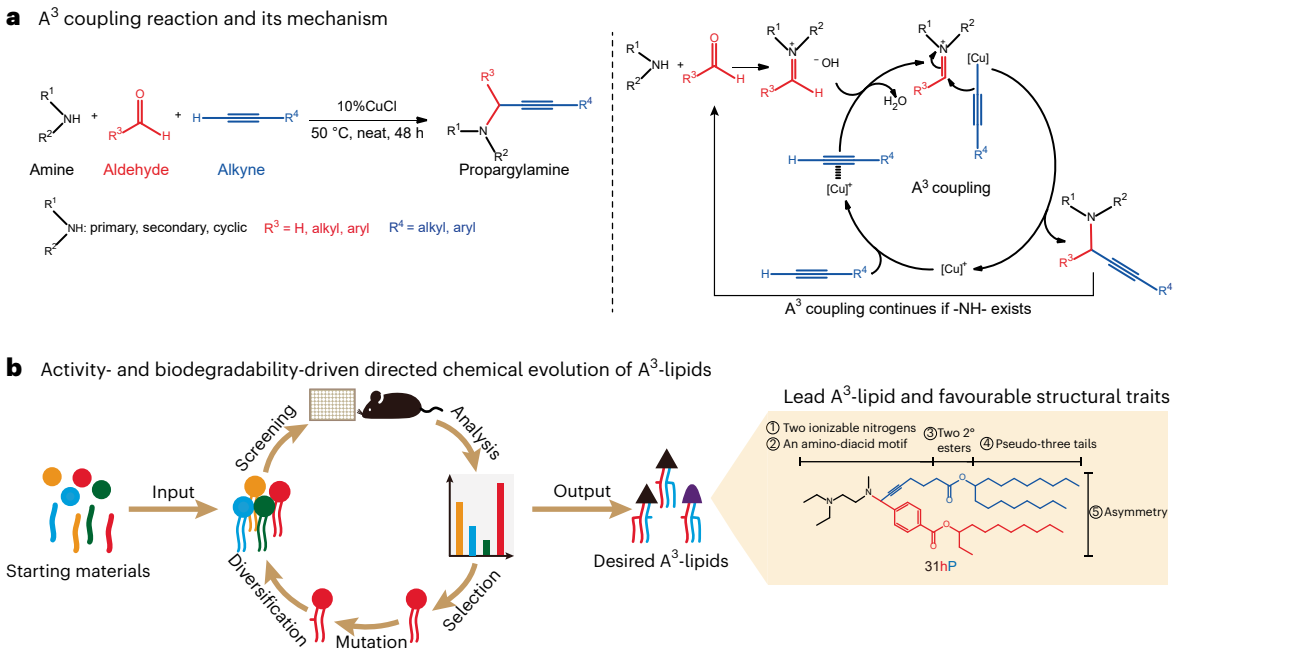

Fig. 1 | A^3-coupling reaction and activity- and degradability-driven directed chemical evolution of A^3-lipids. a, The reaction scheme and mechanism of A^3-coupling. An alkynyl–Cu intermediate is formed, which reacts with in situ produced iminium ion originated from aldehyde and amine to form a propargylamine with concomitant regeneration of the Cu^+ catalyst. **b**, A workflow of activity- and degradability-driven directed chemical evolution of A^3-lipids. The process starts with a pilot library of A^3-lipids established using readily available starting materials. After screening and analysis, the selected A^3-lipid is used as the starting point for subsequent rounds of rationale-driven, customized, site-directed 'mutagenesis' and selection, which gradually improves the desired activity and biodegradability over multiple iterations. This directed chemical evolution approach enables accelerated discovery of desired ionizable lipids and valuable design criteria. The desired A^3-lipids comprise two ionizable nitrogens, an amino-diacid motif, two 2° esters and pseudo-three tails with an asymmetric tail structure.

development of ionizable lipids with improved activity and biodegradability. Ionizable lipids are conventionally synthesized via medicinal chemistry or combinatorial chemistry. The medicinal chemistry approach involves rational design and multistep organic synthesis of ionizable lipids, guided by the putative in vivo mechanism of action and empirical structural criteria[5]. The US Food and Drug Administration (FDA)-approved DLin-MC3-DMA (MC3) is a representative ionizable lipid developed on the basis of this approach[5,6]. Although this approach ensures a high success rate to generate desirable lipid candidates, it is limited by laborious, low-throughput synthesis, making it difficult to create structurally diverse lipids and systematically investigate structure–activity relationships (SARs). The combinatorial chemistry approach typically involves one-pot synthesis of ionizable lipids based on highly efficient two-component reactions or multicomponent reactions (MCRs)[7–11]. It enables rapid, high-throughput synthesis of structurally diverse lipids, yet it suffers from a low hit rate for lipids with both high potency and biodegradability due to limitations regarding readily available starting materials[7,8]. Combining medicinal chemistry-based rational design of optimal building blocks with combinatorial chemistry-based high-throughput synthesis exploits the advantages of both approaches to generate desired ionizable lipid structures[12,13]. However, this combined approach is still highly dependent on user's empiricism and trial-and-error practices, motivating the development of a rationale-driven and stepwise method to structurally optimize ionizable lipids with desired properties.

Directed evolution is a powerful technique used in both chemistry and biology to engineer or improve molecules and biological systems with desired properties by mimicking the principles of natural evolution in a controlled environment[14–16]. This process involves iterative rounds of mutation, screening and selection to optimize the desired traits or functions[15]. We hypothesized that the principles of directed evolution could be harnessed to accelerate ionizable lipid development with improved activity and biodegradability.

In this study, we propose a directed chemical evolution approach for the accelerated, rationale-driven, iterative structural optimization of ionizable lipids based on an innovative combinatorial chemistry—A^3 (amine–aldehyde–alkyne) coupling (Fig. 1a). First, we generated a pilot library of propargylamine-based ionizable lipids (termed A^3-lipids) using commercially available starting materials and then screened these lipids for their mRNA delivery efficacy (Fig. 1b). The top-performing A^3-lipid with favourable structures/traits was used as the starting point for the subsequent round of rationale-driven, customized, site-directed 'mutagenesis' and selection, gradually improving potency and biodegradability over multiple iterations. After five rounds of directed chemical evolution, we discovered dozens of biodegradable, asymmetric A^3-lipids with potencies reaching or surpassing an industry standard ionizable lipid and identified key structural criteria dictating their in vivo mRNA delivery efficacy. Finally, we demonstrated the enhanced performance of our lead A^3-lipid relative to two FDA-approved ionizable lipids, in both mRNA-based gene editing and vaccine applications. We anticipate that our directed chemical evolution methodology and discovered structural criteria can accelerate the development of desirable ionizable lipids for mRNA delivery from potential years to months or even weeks.

Results

Generating A^3-lipids via commercially available starting materials

The three-component coupling of an amine, an aldehyde and an alkyne, commonly known as A^3-coupling, has been established as a one-pot, convenient and general approach towards propargylamine derivatives[17]. This reaction can be performed under ambient, solvent-free conditions with good tolerance of many functional groups (for example,

https://doi.org/10.1038/s41551-024-01267-7

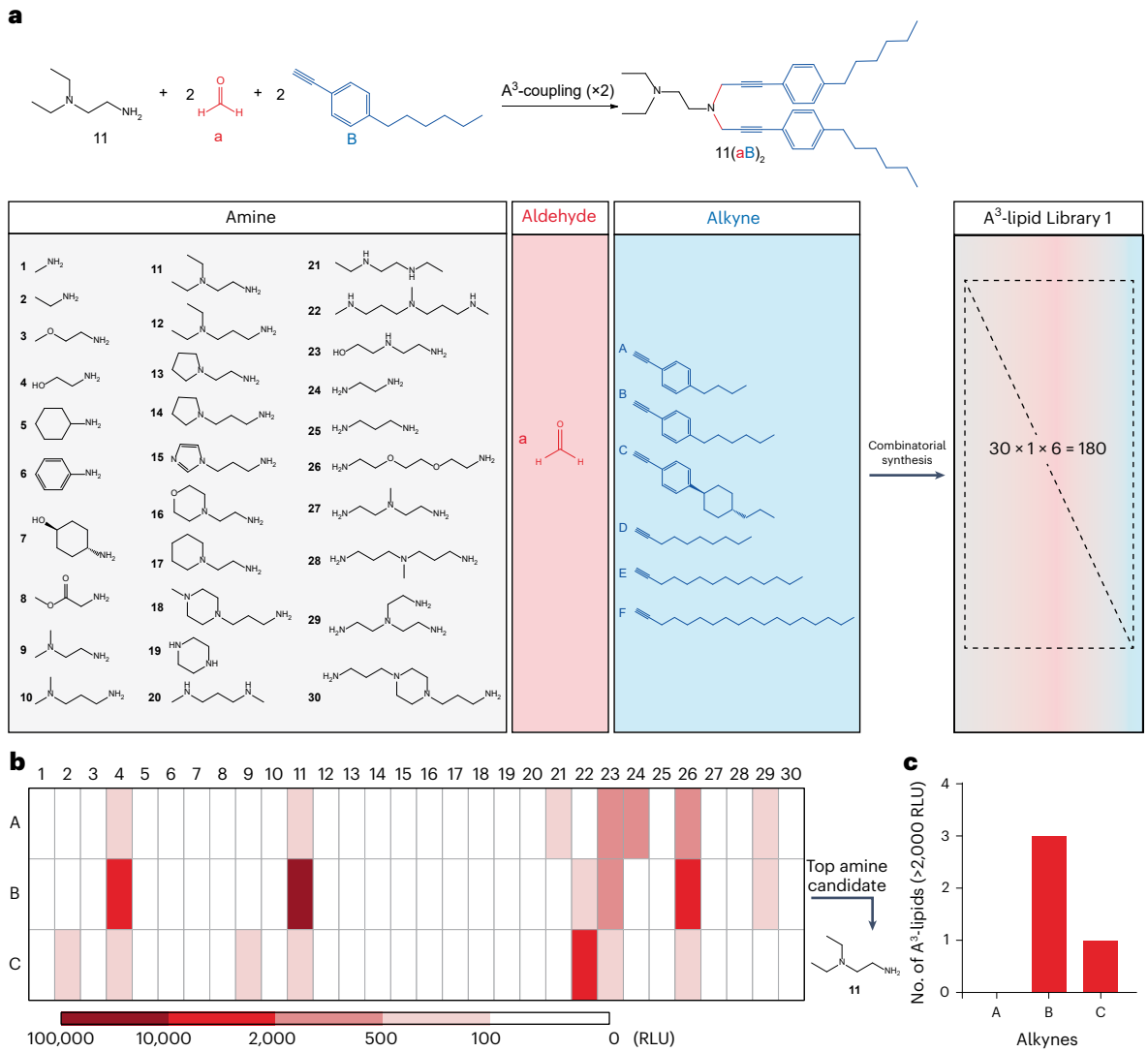

Fig. 2 | Combinatorial synthesis and screening of A^3-lipids in Library 1. **a**, Combinatorial synthesis of A^3-lipids via A^3-coupling of commercially available amines (1–30), formaldehyde (a) and alkynes (A–F). A representative synthesis of 11(aB)$_2$ through A^3-coupling twice is shown. **b**, In vitro mLuc expression in a heat map. Data are presented as mean (n = 2 independent biological replicates, initial screening). HepG2 cells were treated with mLuc-loaded LNPs at an mRNA dose of 15 ng per well for 24 h. RLU, relative light unit. Untreated cells typically exhibited <100 RLU. **c**, Distribution of A^3-lipids with in vitro mLuc expression >2,000 RLU across alkyne structure.

alcohols, carboxylic acids and esters)[18]. A^3-coupling is atom economical and eco-friendly with water as the only by-product[19]. Moreover, depending on the amine and aldehyde used, symmetric dipropargylamines or asymmetric monopropargylamines can be synthesized, which increases the structural diversity of the products. Therefore, A^3-coupling is an ideal combinatorial chemistry reaction for ionizable lipid synthesis.

Since A^3-coupling has never been adapted for synthesizing ionizable lipids, we first established a pilot library of 180 A^3-lipids to evaluate the potential of this reaction using commercially available amines (1–30), formaldehyde (a) and alkynes (A–F) (Fig. 2a). Notably, excess aldehyde and alkyne were used to enable repeated A^3-coupling to produce tertiary (3°) amine-based A^3-lipids (Supplementary Fig. 1). We noticed that aromatic alkynes (A–C) typically gave moderate yields (~50%), whereas aliphatic alkynes (D–F) typically gave poor yields (<10%). This observation is consistent with previous studies, where aliphatic alkynes were found to be less efficient in forming dipropargylamines compared with aromatic alkynes[18,20].

We next proceeded to test the in vitro mRNA delivery efficiency of 90 A^3-lipids derived from aromatic alkynes due to their practical yields (Fig. 2b). In vitro testing, which has been widely used to screen large libraries of crude ionizable lipids[7,12], allows us to preliminarily identify promising lipid candidates, exclude inefficacious ones and understand SARs in a time- and resource-efficient manner. Crude A^3-lipids were formulated into A^3-LNPs along with other standard lipid excipients and firefly luciferase mRNA (mLuc). HepG2 cells (a human hepatocellular carcinoma cell line) were treated with A^3-LNPs at a low mRNA dose (15 ng per well) to avoid potential cytotoxicity (Supplementary Fig. 2). Among the A^3-lipids in this library, amine 11-derived symmetric 11(aB)$_2$ demonstrated the highest transfection, and its analogues (that is, 11(aA)$_2$ and 11(aC)$_2$) also showed some transfection (>100 RLU, Fig. 2b). Notably, the alkyl substituent on the aromatic alkyne greatly affected mRNA transfection, and the elongation of the alkyl substituent appeared to increase the delivery efficiency (Fig. 2c). Through this pilot study, we quickly validated the feasibility of A^3-coupling to produce ionizable lipids and the potential of amine 11-based A^3-lipids for mRNA delivery. However, the lead A^3-lipid 11(aB)$_2$ is not optimal for in vivo mRNA delivery applications since it is not biodegradable and contains relatively short tails compared with FDA-approved ones[1,6].

https://doi.org/10.1038/s41551-024-01267-7

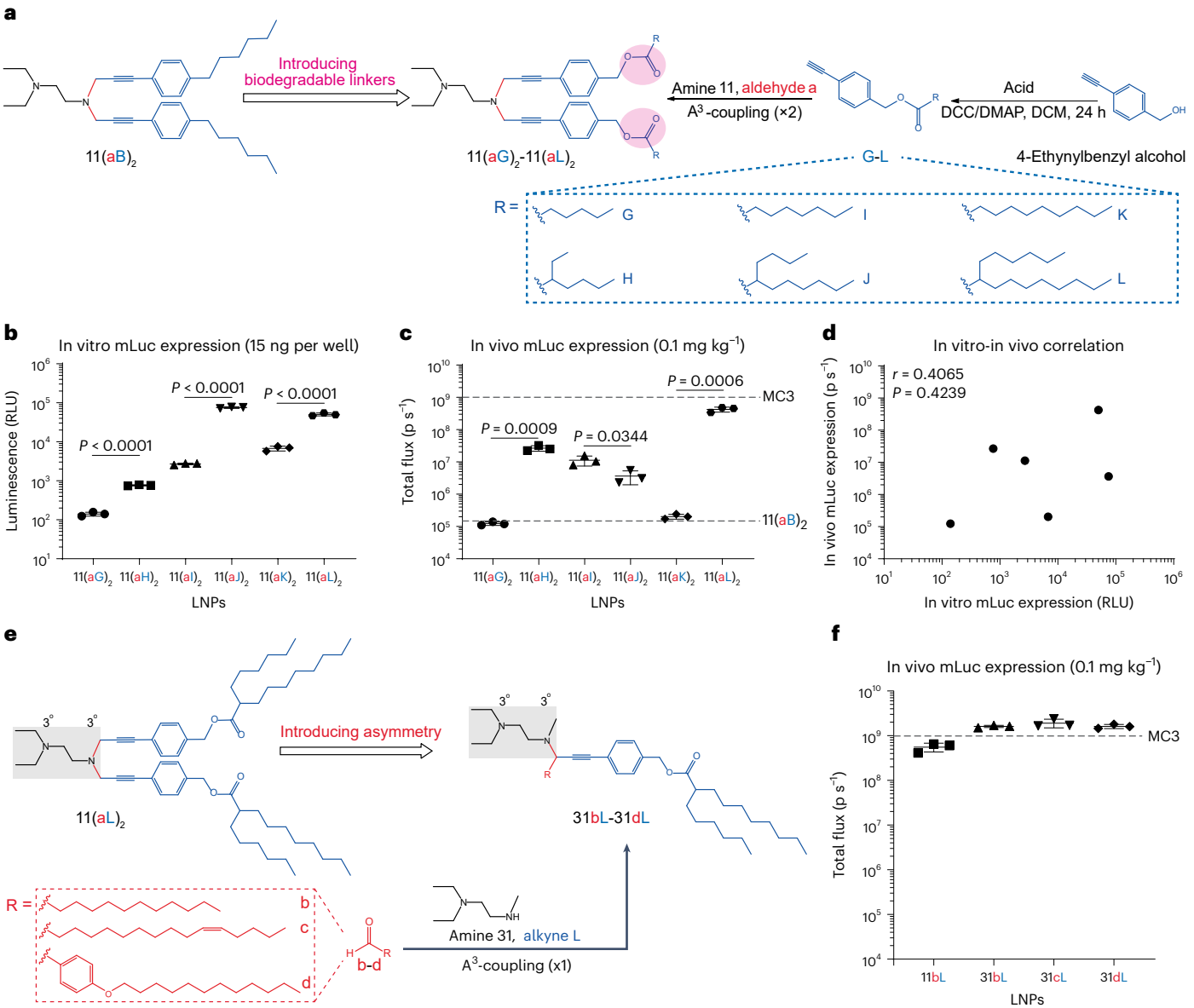

Fig. 3 | Optimization of symmetric A^3-lipids with biodegradable alkynes in Library 2 and asymmetric A^3-lipids with long-chain aldehydes in Library 3. **a**, Biodegradability-driven directed chemical evolution of A^3-lipids starting from 11(aB)$_2$. Cleavable ester linkers were introduced into 11(aB)$_2$ and 6 biodegradable symmetric A^3-lipids with linear or branched tails were generated. **b**, In vitro mLuc expression. HepG2 cells were treated with mLuc-loaded LNPs at an mRNA dose of 15 ng per well for 24 h. Data are presented as mean ± s.d. (n = 3 independent biological replicates). Statistical significance was evaluated using one-way ANOVA with Tukey's correction. **c**, In vivo mLuc expression. Mice were i.v. injected with mLuc-loaded LNPs at an mRNA dose of 0.1 mg kg^{-1}. Images were taken at 4 h post treatment and whole-body total flux was quantified. Dashed lines indicate the levels of 11(aB)$_2$ LNP and MC3 LNP, respectively. Data are presented as mean ± s.d. (n = 3 independent biological replicates). Statistical significance was evaluated using one-way ANOVA with Tukey's correction. **d**, Correlation between in vitro and in vivo mLuc expression. Statistical significance was evaluated using two-tailed correlation analysis in GraphPad Prism 8.0. **e**, Asymmetry-driven directed chemical evolution of A^3-lipids starting from 11(aL)$_2$. The optimized ionizable head structure (highlighted in grey) and one alkynyl tail L were maintained, while a long-chain aldehyde was introduced as another tail to generate asymmetric A^3-lipid. **f**, In vivo mLuc expression. Mice were i.v. injected with mLuc-loaded LNPs at an mRNA dose of 0.1 mg kg^{-1}. Images were taken at 4 h post treatment and whole-body total flux was quantified. Data are presented as mean ± s.d. (n = 3 independent biological replicates).

Mutating symmetric A^3-lipids via biodegradable alkynes

On the basis of the high in vitro transfection efficacy, we chose 11(aB)$_2$ as the starting point for iterative directed chemical derivatization to optimize the structure. In this cycle, we considered both efficacy and biodegradability, since biodegradable ionizable lipids are highly preferred for in vivo mRNA delivery[1]. Therefore, we introduced cleavable ester linkers into the tail region of A^3-lipids by customizing six aromatic alkynes (G–L) via a one-step esterification reaction (Supplementary Method 1 and Fig. 3a). G, I and K were aromatic alkynes with elongated linear alkyl substituents, while H, J and L were their branched counterparts. Branched alkynyl tails were included since branching allows the ionizable lipid to adopt a more cone-shaped structure that is beneficial for endosomal escape and mRNA delivery[21–23].

The six customized biodegradable A^3-lipids (11(aG)$_2$–11(aL)$_2$, Supplementary Fig. 3) were purified (Supplementary Fig. 4) and tested for in vitro and in vivo mLuc delivery. With increasing tail length and branching, A^3-lipids generally showed increased in vitro transfection efficacy (Fig. 3b and Supplementary Fig. 5), but their in vivo activities

were disparate (Fig. 3c). Linear 11(aG)$_2$ and 11(aK)$_2$ showed limited in vivo transfection efficacy that was similar to that of 11(aB)$_2$, presumably due to their low and high lipophilicity, respectively. Branched A^3-lipids generally outperformed their linear counterparts both in vitro and in vivo, apart from 11(aJ)$_2$ which showed slightly lower in vivo activity than 11(aI)$_2$. 11(aL)$_2$ with a symmetric structure and two biodegradable branched tails was identified as the lead A^3-lipid in this library with the highest in vivo mRNA delivery efficiency. After analysing the relationship between in vitro and in vivo results, we found a poor correlation (Fig. 3d), which has also been observed by others[24]. Therefore, only the in vivo mRNA delivery efficiency of A^3-lipids was examined in subsequent directed chemical evolution cycles.

Mutating asymmetric A^3-lipids via long-chain aldehydes

While the lead 11(aL)$_2$ achieved a whole-body total flux of ~4.2×10^8 p s^{-1}, it did not reach the transfection level of the industry standard lipid MC3, which has been predetermined to be ~1.0×10^9 p s^{-1} (Fig. 3c). Previous studies have suggested that asymmetric ionizable lipids with two different alkyl tails are prone to show better in vivo delivery efficacy than their symmetric analogues[25,26]. It is hypothesized that asymmetric tails lower the packing density, mitigate the crystallization tendency and increase the fluidity of the lipid bilayer[25,27]. Therefore, for the next round of directed chemical evolution, we maintained the optimized ionizable head structure and alkynyl tail L (tail one) while mutating the aldehyde (tail two) to generate asymmetric A^3-lipids.

Notably, owing to the flexibility of A^3-coupling, asymmetric A^3-lipids can be easily synthesized from an amine, a long-chain aldehyde and a long-chain alkyne via A^3-coupling once. To maintain the optimized ionizable head structure, we used a secondary (2°) amine 31 (a methyl derivative of amine 11) to ensure that only 3° amines exist in the A^3-lipid structure (Fig. 3e). Three commercially available long-chain aldehydes (b–d) were used to establish a pilot library of asymmetric A^3-lipids to verify our hypothesis (Supplementary Fig. 6). Excitingly, all three A^3-lipids (31bL–31dL) slightly surpassed the in vivo performance of MC3, with 31cL identified as the lead lipid (Fig. 3f). These data demonstrate the merit of an asymmetric A^3-lipid structure. Moreover, asymmetric A^3-lipids appear to have good tolerability of aldehydes as both aliphatic and aromatic ones can afford potent A^3-lipids.

We also synthesized an asymmetric, 2° amine-containing A^3-lipid 11bL via A^3-coupling once of amine 11, aldehyde b and alkyne L (Supplementary Fig. 6). However, 11bL neither outperformed MC3 lipid nor its 3° amine-containing analogue 31bL (Fig. 3f). Due to the scope of this study, we focused subsequent rounds of directed chemical evolution on the asymmetric, 3° amine-based A^3-lipids.

Mutating asymmetric A^3-lipids via biodegradable aldehydes and alkynes

Inspired by our findings on asymmetric A^3-lipid performance, we further optimized amine 31-based asymmetric A^3-lipids by introducing biodegradability into the aldehyde structure and diversifying the tail structures. In this cycle of directed chemical derivatization, five biodegradable aromatic aldehydes (e–i) with linear or branched structures were synthesized via a one-step esterification reaction (Supplementary Method 1 and Fig. 4a). Here we chose aromatic aldehydes for two reasons: first, they can be easily prepared; second, the benzylic structure is indicated to enhance the stability of LNP through intermolecular π − π stacking[28]. Similarly, we synthesized six additional biodegradable alkynes (M–R) with linear or branched structures. Notably, we diversified these aldehydes and alkynes using different lengths of branch chain (for example, h vs i) and ester orientation (for example, M vs Q) to study their SARs. Through combinatorial synthesis, 35 asymmetric A^3-lipids were generated in this library (Fig. 4a and Supplementary Fig. 7). In contrast to Library 1, here we found that aliphatic alkynes (M–R) gave moderate yields (~50%) similar to that of the aromatic alkyne L, likely because only a single A^3-coupling reaction was required to afford these monopropargylamine products.

After screening the in vivo mLuc delivery activity of Library 4, we identified eight asymmetric A^3-lipids with transfection efficacy greater than that of MC3 lipid (Fig. 4a and Supplementary Fig. 8). Specifically, four asymmetric A^3-lipids (31iN, 31iO, 31gP and 31 hP) facilitated more than 5-fold greater luciferase expression relative to MC3, with 31hP identified as the top-performer (8-fold higher). Of note, all these four A^3-lipids comprise an amino-diacid motif, two 2° esters and two major tails with one long branch tail (pseudo-three tails). Deviating from these structural criteria generally led to reduced in vivo activity (Fig. 4a). The potency of our lead A^3-lipids is supported by previous studies that have shown that (1) 2° esters show slower degradation than primary ones, prolonging the availability of the mRNA–LNP complex[22,26]; (2) branched tail structures allow the ionizable lipid to adopt a more cone-shaped structure for enhanced endosomal disruption[23,29]; (3) negatively charged carboxylates attached to the ionizable headgroup can neutralize the positive charge, facilitating accelerated dissociation of the mRNA–LNP complex and release of mRNA[30].

Mutating the headgroup of asymmetric A^3-lipids

With the optimal linker and tail structure identified, we revisited the ionizable headgroup in our final cycle of directed chemical evolution. We mutated the headgroup while maintaining the optimal tail region as 'hP', and screened 26 additional 2° amines with only one active site (–NH–) for the A^3-coupling reaction (Fig. 4b and Supplementary Fig. 9). These structurally diverse amines contain different numbers (0–2) of ionizable nitrogens. To the best of our knowledge, most of these amines have not been previously tested.

In this library, we discovered 11 more asymmetric A^3-lipids that reached the transfection efficacy of MC3 lipid (Fig. 4b). However, none of these A^3-lipids surpassed the potency of 31hP including the lead 32hP, suggesting the superiority of amine 31 for mRNA delivery. Interestingly, two ionizable nitrogens occurred in all potent A^3-lipids (31–42 hP), but this feature alone was not adequate to afford potent ones (for example, 43hP, 45–49hP). A^3-lipids with one ionizable nitrogen (51hP, 54–57hP) or three ionizable nitrogens (44hP, 50hP and 52hP) were inferior for in vivo mRNA delivery, which may be a detrimental consequence of dramatically changed polarity.

After five cycles of activity- and biodegradability-driven directed chemical evolution of A^3-lipids, we identified 31hP as the top-performing ionizable lipid (characterization data in Supplementary Figs. 4, 10 and 11). Notably, throughout this process, we found that 31hP LNP and other potent A^3-LNPs predominantly transfected the liver upon intravenous (i.v.) administration, which is consistent with MC3 LNP and the majority of LNPs reported in the literature (Supplementary

Fig. 4 | Optimization of biodegradable tails and headgroups for asymmetric A^3-lipids in Libraries 4 and 5. a, Optimization of biodegradable tails in asymmetric A^3-lipids in Library 4. A total of 35 asymmetric A^3-lipids were combinatorially synthesized via A^3-coupling of amine 31, 5 biodegradable aldehydes (e–i) and 7 biodegradable alkynes (L–R). A representative synthesis of 31hP through A^3-coupling is shown. Mice were i.v. injected with mLuc-loaded LNPs at an mRNA dose of 0.1 mg kg^{-1}. Images were taken at 4 h post treatment and whole-body total flux was quantified. Data are presented as mean ($n = 3$ independent biological replicates). **b**, Screening of ionizable headgroup in asymmetric A^3-lipids in Library 5. A total of 26 asymmetric A^3-lipids were combinatorially synthesized via A^3-coupling of secondary amine (32–57), aldehyde h and alkyne P. Mice were i.v. injected with mLuc-loaded LNPs at an mRNA dose of 0.1 mg kg^{-1}. Images were taken at 4 h post treatment and whole-body total flux was quantified. Data are presented as mean ± s.d. ($n = 3$ independent biological replicates). **c**, Structure (left) and in vivo mRNA delivery activity (right) of lead A^3-lipid in each library. Data are presented as mean ± s.d. ($n = 3$ independent biological replicates). Statistical significance was evaluated using one-way ANOVA with Tukey's correction.

https://doi.org/10.1038/s41551-024-01267-7

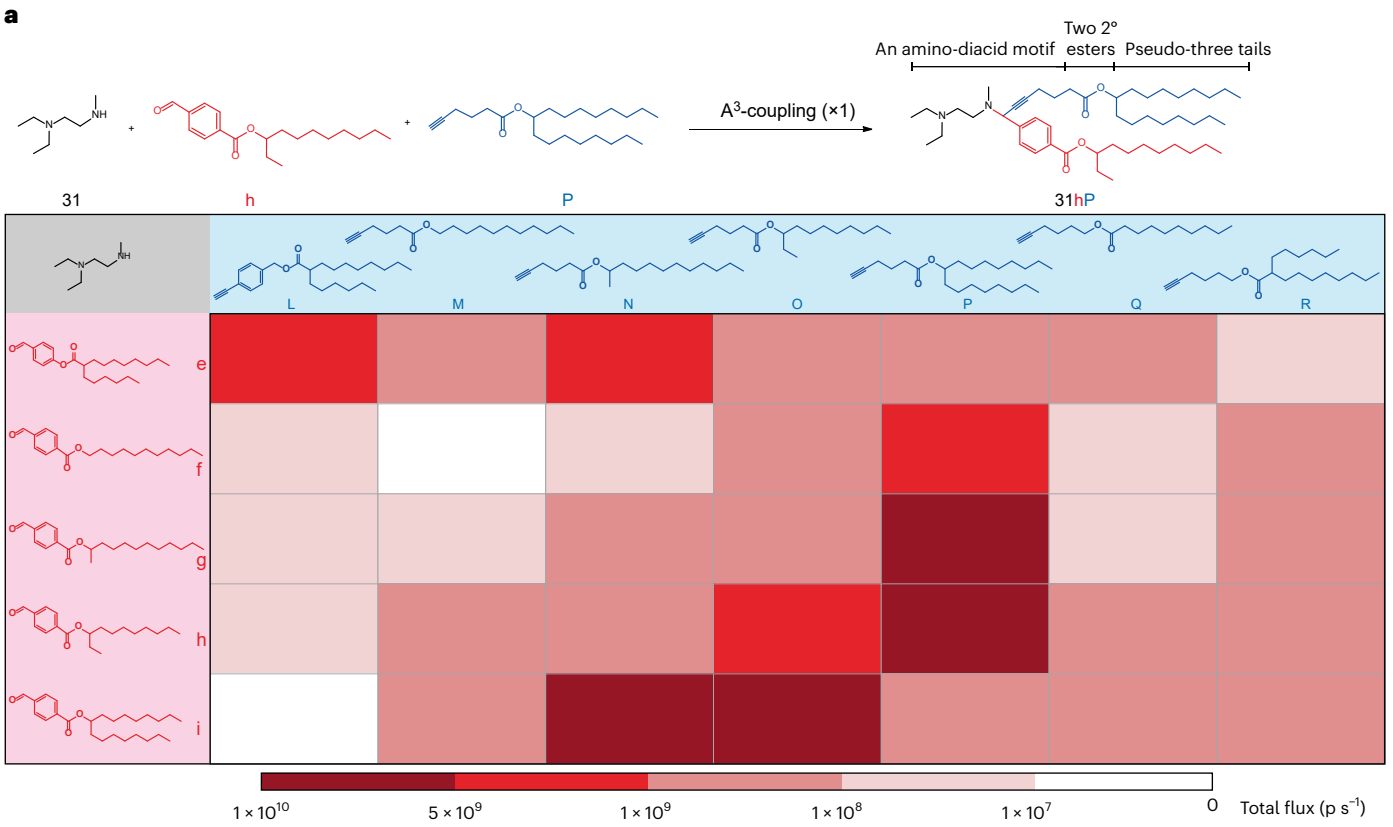

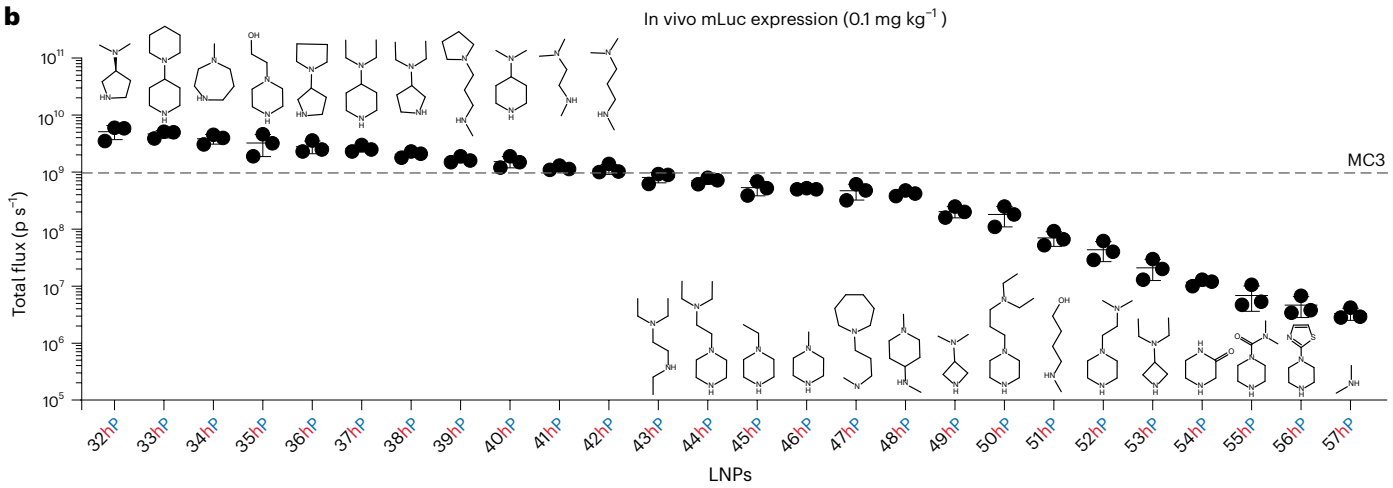

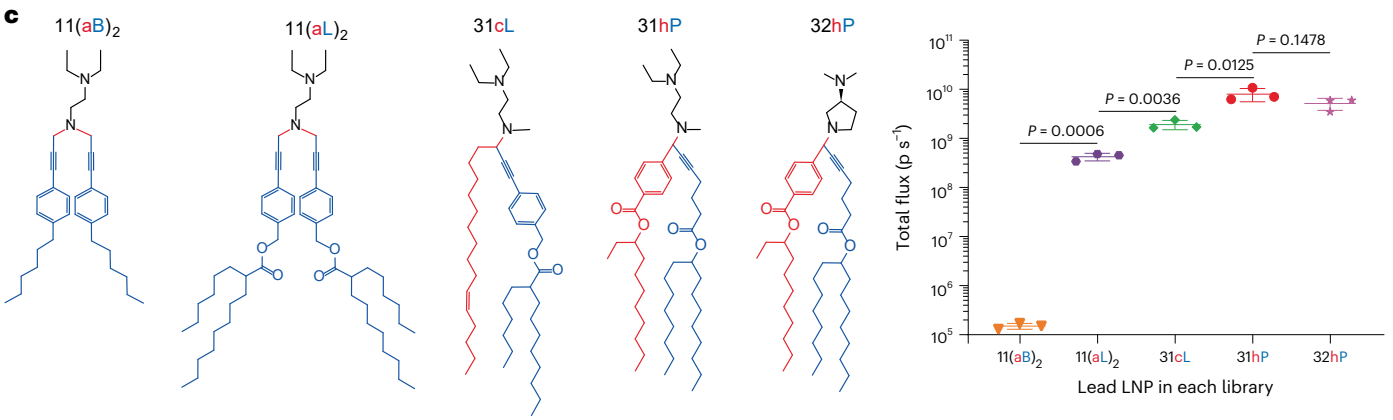

Table 1 | Summary of five cycles of activity- and degradability-driven directed chemical evolution of A^3-lipids

Library	Design rationale	Favourable structure/trait	Lead A^3-lipid	No. of degradable linkers	Activity (ps^{-1})
1	Commercial availability and diversity of building blocks	Amine 11; longer alkyl substituent	$11(aB)_2$	0	$(1.5\pm0.2)\times10^5$
2	Length, branching and biodegradability of tail	Alkyne L; branched tail	$11(aL)_2$	2	$(4.2\pm0.7)\times10^8$
3	3° amine; asymmetry and commercial availability of tail	Amine 31; asymmetric tails	31cL	1	$(1.9\pm0.4)\times10^9$
4	Biodegradability and branching of tail; ester orientation	Tail region 'hP'; an amino-diacid motif; two 2° esters; pseudo-three tails	31hP	2	$(8.0\pm2.4)\times10^9$
5	Diversity of headgroup; number of ionizable nitrogens	Two ionizable nitrogens	32hP	2	$(5.1\pm1.4)\times10^9$

Data are presented as mean±s.d. (n=3 independent biological replicates).

Fig. 12). Moreover, we confirmed that 31hP could be rapidly degraded in the presence of esterase owing to two biocleavable ester bonds (Supplementary Fig. 13), which exhibited improved biodegradability compared with MC3 and comparable biodegradability relative to SM-102 (an asymmetric ionizable lipid with similar ester orientation and pseudo-three tails to our 31h that is used in Moderna's mRNA-1273 vaccine). It is worth mentioning that, during this process, we rationally designed the following library on the basis of the lead A^3-lipid and favourable structures/traits identified in the last library and introduced proper 'mutagenesis', so we could direct the chemical evolution of A^3-lipids towards this desired outcome (Fig. 4c and Table 1).

Characterization of A^3-LNPs

We next characterized the physicochemical properties of the top-performing 31hP LNP formulated by microfluidic mixing (Fig. 5a). The hydrodynamic size of 31hP LNP was ~80 nm with a polydispersity index (PDI) of 0.093 and a neutral surface charge ($\zeta = -0.27$ mV). The mRNA encapsulation efficiency (EE) was determined to be ~93%. The apparent pK_a (acid dissociation constant) of LNP was determined to be 6.25 (Supplementary Fig. 14). Owing to its ionization property, 31hP LNP showed good haemocompatibility at pH 7.4 and increased haemolysis at pH 6.0 (Supplementary Fig. 15). Cryogenic electron microscopy (cryo-EM) imaging results showed that 31hP LNP had a dense spherical structure with a lamellar shell and an amorphous core (Fig. 5b). To investigate the key pathways governing the cellular uptake of 31hP LNP, we performed an internalization inhibition study in vitro (Fig. 5c). The transfection efficacy was significantly reduced in the presence of amiloride or methyl-β-cyclodextrin (Mβ-CD), suggesting that the cellular uptake of 31hP LNP is mainly facilitated through macropinocytosis and lipid raft-mediated endocytosis.

We further evaluated the stability of 31hP LNP (Supplementary Fig. 16a–c). At 1 week post storage at 4 °C, the hydrodynamic size and PDI of 31hP LNP increased minimally, suggesting its good colloidal stability. Moreover, the in vivo transfection potency of 31hP only moderately decreased (Supplementary Fig. 16d,e). In comparison, both MC3 LNP and SM-102 LNP showed increased size and PDI with a substantial decrease in in vivo transfection potency. It is hypothesized that the benzylic linker contributes to the assembly and stability of 31hP LNP through intermolecular π − π stacking (Supplementary Fig. 17), which have been utilized in the design of a stable one-component nanoparticle mRNA delivery system[28].

Delivering mRNA-based gene editors and vaccines using A^3-LNPs

Following characterization, we aimed to demonstrate the utility of our A^3-lipids by delivering therapeutic mRNAs. The 31hP LNP was first examined for the hepatic delivery of mRNA-based CRISPR gene editors, which are much larger than mLuc (~2,000 nt) and are challenging to deliver in vivo[31]. Four other lead A^3-LNPs (that is, $11(aB)_2$ LNP, $11(aL)_2$ LNP, 31cL LNP and 32hP LNP) selected from each library were also tested to verify our directed chemical evolution approach, and liver-tropic MC3 LNP was selected as the industry standard control LNP (Supplementary Table 1). In a proof-of-principle study, we formulated LNPs co-encapsulating Cas9 mRNA (~4,500 nt) and a single guide RNA (sgRNA) (~100 nt) specific for the transthyretin (TTR) gene, which is implicated in hereditary amyloidosis[32]. A single injection of 31hP LNP co-delivering Cas9 mRNA and TTR sgRNA at a total RNA dose of 1 mg kg^{-1} achieved ~18% on-target editing at the TTR locus in the liver and ~30% serum TTR reduction (Fig. 5d–f), which were significantly higher than those of MC3 LNP and other A^3-LNPs. Importantly, the TTR gene editing efficiency of A^3-LNPs correlated well with in vivo mLuc expression (Fig. 5g), proving the rationale of our directed chemical evolution approach based on mLuc delivery to improve the activity of the ionizable lipid. We further examined some inferior A^3-LNPs (that is, $11(aK)_2$ LNP, 11bL LNP and 31hR LNP) that were excluded during our directed chemical evolution as well as another industry LNP (that is, LP01 LNP) containing a biodegradable, asymmetric ionizable lipid LP01 (Supplementary Table 1)[32]. We found that none of these LNPs outperformed 31hP LNP in terms of TTR gene editing and serum TTR reduction (Supplementary Fig. 18), which further demonstrated the superiority of our approach and 31hP.

Next, we investigated the hepatotoxicity of A^3-LNPs following gene editing. Unlike $11(aB)_2$ LNP and 31cL LNP, A^3-LNPs formulated with A^3-lipids with two biodegradable tails (that is, $11(aL)_2$ LNP, 31hP LNP and 32hP LNP) were well tolerated in mice, with no abnormal increases in alanine transaminase (ALT) and aspartate aminotransferase (AST) at 24 h post treatment (Supplementary Fig. 19), demonstrating the rationale of our approach to improve ionizable lipid safety by introducing more biodegradable linkers. In particular, we examined the hepatotoxicity of the degradation metabolite of 31hP (that is, 31hP-M, Supplementary Method 2 and Supplementary Fig. 19) as well as the immunotoxicity of 31hP LNP (Supplementary Fig. 20). With no major toxicity observed, we confirmed a good safety profile of 31hP LNP.

Finally, we evaluated 31hP LNP for mRNA vaccine applications. Recently, the FDA approved the Moderna SARS-CoV-2 mRNA–LNP vaccine that uses the SM-102 ionizable lipid. Therefore, we compared the immunogenicity of SARS-CoV-2 Spike mRNA-loaded 31hP LNP and SM-102 LNP after intramuscular (i.m.) vaccination (Fig. 5h). In a standard prime–boost rodent vaccine model, 31hP LNP elicited a significantly higher anti-Spike antibody titre than the SM-102 LNP vaccine (Fig. 5i). Using a lentivirus-based SARS-CoV-2 pseudovirus neutralization assay, we further confirmed that 31hP LNP triggered a significantly higher neutralization antibody titre than SM-102 LNP (Fig. 5j). Notably, $11(aL)_2$ LNP, 31cL LNP and 32hP LNP triggered higher antibody responses than SM-102 LNP as well. Interestingly, these A^3-LNPs and 31hP LNP enabled comparable protein expression to SM-102 LNP in the muscle (Fig. 5k and Supplementary Fig. 21), suggesting that other factors (for example, adjuvant effects) might contribute to the

https://doi.org/10.1038/s41551-024-01267-7

a

LNP	31hP LNP
Size (nm)	79.3 ± 5.1
PDI	0.093
Zete potential (mV)	−0.27 ± 0.03
EE (%)	92.9 ± 1.5
p*K*a	6.25

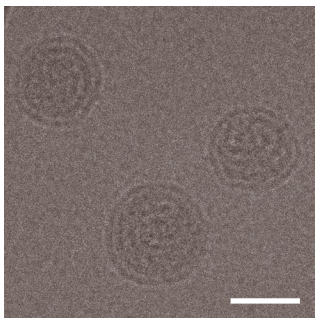

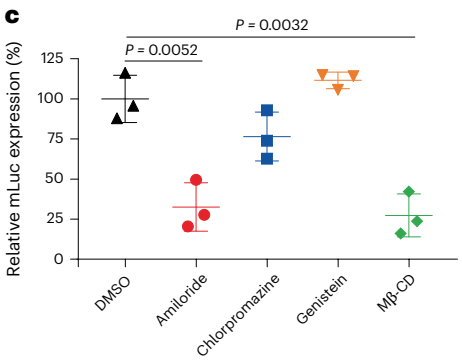

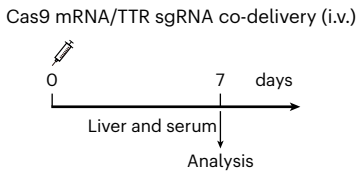

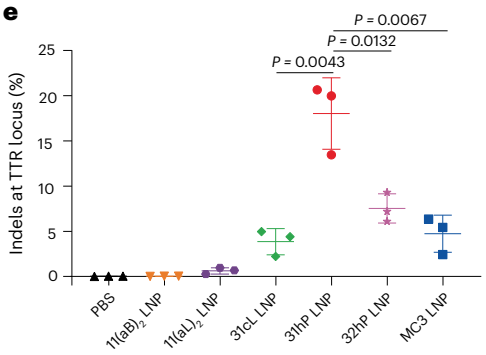

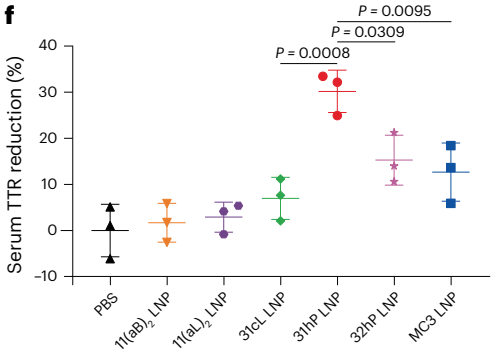

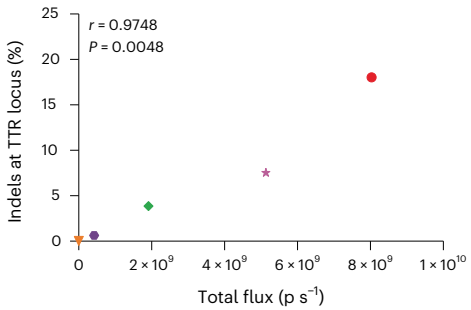

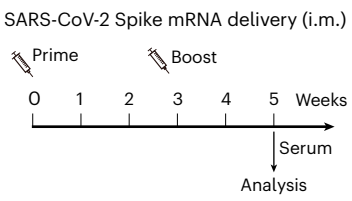

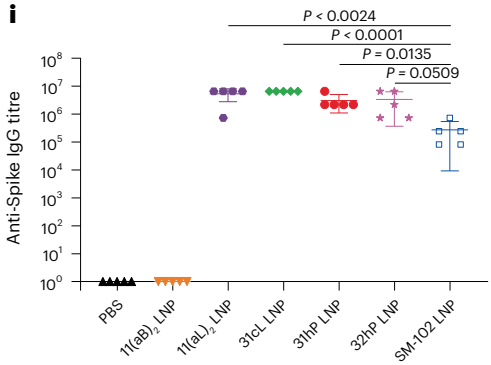

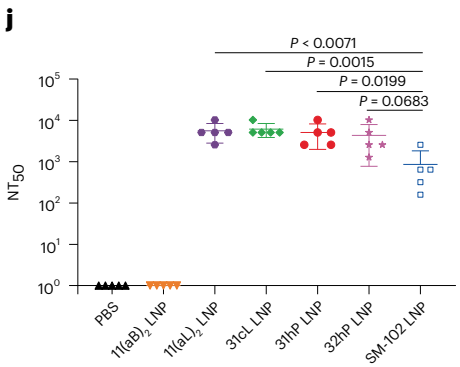

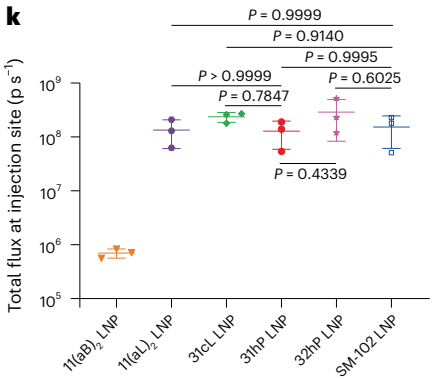

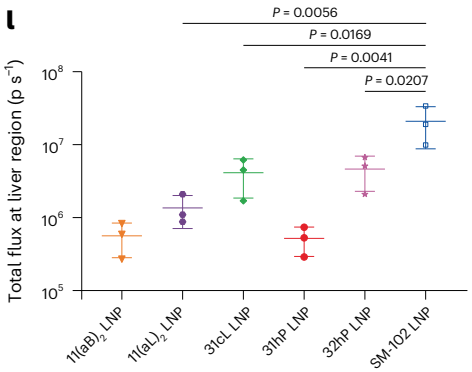

significantly higher immunogenicity of our A^3-LNPs[10,33,34]. Moreover, these A^3-LNPs mediated significantly less off-target expression in the liver relative to SM-102 LNP (Fig. 5l), which can potentially mitigate adverse effects (for example, liver injury) associated with current mRNA–LNP vaccines[35].

Taken together, these results demonstrate the utility of our activity- and biodegradability-driven directed chemical evolution approach to optimize ionizable lipids towards a desired outcome. Moreover, these results strongly support that 31hP is a superior ionizable lipid relative to industry standard ionizable lipids and holds great promise in the systemic delivery of mRNA therapeutics and intramuscular delivery of mRNA vaccines.

Discussion

Although extensive efforts have been put into the development of ionizable lipids through rational design and/or combinatorial synthesis, there is a lack of methods for stepwise, rational optimization of ionizable lipid structure. In the majority of studies in the literature, researchers typically created a single library of ionizable lipids and investigated SARs. Ionizable lipids generated through this strategy are usually associated

Fig. 5 | Characterization of A^3-LNP and its application in delivering mRNA-based gene editors and vaccines. a, Physicochemical parameters of 31hP LNP formulated by microfluidic mixing. Data are presented as mean ± s.d. ($n = 3$ independent biological replicates). **b**, A representative cryo-EM image of 31hP LNP. Scale bar, 50 nm. **c**, In vitro transfection of 31hP LNP in the presence of various endocytic inhibitors. Amiloride, an inhibitor of macropinocytosis; chlorpromazine, an inhibitor of clathrin-mediated endocytosis; genistein, an inhibitor of caveolae-mediated endocytosis; Mβ-CD, an inhibitor of lipid raft-mediated endocytosis. Data are presented as mean ± s.d. ($n = 3$ independent biological replicates). Statistical significance was evaluated using one-way ANOVA with Tukey's correction. **d**, A scheme of LNP-enabled co-delivery of Cas9 and TTR sgRNA. Mice were i.v. injected with LNPs encapsulating Cas9 mRNA/TTR sgRNA (4:1, w/w) at a total RNA dose of 1 mg kg^{-1}. On day 7, DNA was extracted from the liver to determine on-target indel frequency using NGS, and serum was collected to determine TTR concentration using ELISA. **e**, Indels at TTR locus. Data are presented as mean ± s.d. ($n = 3$ independent biological replicates). Statistical significance was evaluated using one-way ANOVA with Tukey's correction. **f**, Serum TTR. Data are presented as mean ± s.d. ($n = 3$ independent biological replicates). Statistical significance was evaluated using one-way ANOVA with Tukey's correction. **g**, Correlation between in vivo mLuc expression and TTR gene editing efficiency. Statistical significance was evaluated using two-tailed correlation analysis in GraphPad Prism 8.0. **h**, A scheme of LNP-enabled delivery of SARS-CoV-2 Spike mRNA vaccine. Mice were vaccinated i.m. at a dose of 2 μg mRNA per mouse twice using a prime–boost strategy at a 3-week interval. Serum was collected at the indicated time points to determine anti-Spike IgG titres and SARS-CoV-2 pseudovirus neutralization antibody titres. **i**, Anti-Spike IgG titres. Data are presented as mean ± s.d. ($n = 5$ independent biological replicates). Statistical significance was evaluated using one-way ANOVA with Tukey's correction. **j**, SARS-CoV-2 pseudovirus NT_{50}. Data are presented as mean ± s.d. ($n = 5$ independent biological replicates). Statistical significance was evaluated using one-way ANOVA with Tukey's correction. **k**,**l**, In vivo mLuc expression following i.m. administration. Mice were i.m. injected with mLuc-loaded LNPs at a dose of 2 μg mRNA per mouse. Images were taken at 4 h post treatment and total flux at injection site (**k**) or liver region (**l**) was quantified. Data are presented as mean ± s.d. ($n = 3$ independent biological replicates). Statistical significance was evaluated using one-way ANOVA with Tukey's correction.

with suboptimal structures and properties, and further optimization and iteration is typically conducted and reported years later in subsequent work. For example, Cullis and colleagues iterated on their first reported ionizable lipid DODAP to DLin-KC2-DMA to MC3 and to L319 with increased potency and biodegradability in separate studies over the course of 10 years[5,6,30,36]. Similarly, Moderna developed lipid 5 to lipid H (SM-102) and then to their newest lead candidate lipid 29 over the course of several years[26,37,38].

Directed evolution is a powerful, high-throughput engineering approach that has been successfully utilized to generate adeno-associated viruses with enhanced transduction efficiency and tissue tropism[39,40]. Inspired by this, we hypothesized that directed chemical evolution of ionizable lipids could be achieved through multiple rounds of rationale-driven, customized, site-directed mutation and selection under the selective pressure of transfection efficacy and biodegradability. With the help of this methodology, we can guide ionizable lipid evolution towards a desired outcome with a dramatically truncated timeline from potential years to months or even weeks, in contrast to the conventional paradigm for ionizable lipids iteration in a prolonged timeline and a low-efficiency manner.

In our study, this process began by creating a pilot library of A^3-lipids using diverse, commercially available building blocks. We conducted this pilot study to evaluate the feasibility, gather preliminary data and identify potential issues. In Library 2, we introduced rationale-driven, customized, site-directed 'mutagenesis'—biodegradable ester linkers and branches—into the backbone of the selected $11(aB)_2$ lipid, leading to the identification of a biodegradable symmetric lipid $11(aL)_2$. In Library 3, we introduced asymmetry into the selected $11(aL)_2$ lipid and created a pilot library of asymmetric A^3-lipids using commercially available long-chain aldehydes. After the successful verification of our hypothesis about asymmetry, we further expanded the diversity of asymmetric A^3-lipids in Library 4 by introducing rationale-driven, customized 'mutagenesis'—biodegradable ester linkers, branches and aliphatic alkynes. In Library 5, we kept the optimal tail region constant and mutated the headgroup using various amines to further gain insights into this ionizable motif. Importantly, this directed chemical evolution of A^3-lipids can be continued on the basis of varying research interests. For example, to investigate the positional effect of the ester linkage[26,30], customized ester 'mutagenesis' can be introduced into different positions of the long-chain aldehydes and alkynes. In addition, ionizable lipids containing 2° amines have demonstrated superior in vivo activity in some studies[7,8], therefore, we can also choose 11bL as the starting point for subsequent rounds of directed chemical evolution to optimize A^3-lipids with this trait.

Here, A^3-coupling was adapted to synthesize symmetric and asymmetric ionizable lipids. We found this synthetic method to be a particularly useful MCR to generate asymmetric ionizable lipids with two distinct tails, which typically require laborious synthesis[26,41,42]. Moreover, the mild synthetic conditions, easily accessible building blocks, good tolerance of functional groups and minimal by-products make A^3-coupling an ideal combinatorial chemistry for ionizable lipid synthesis. In addition, due to the nature of A^3-coupling, all synthesized A^3-lipids contain an alkyne structure, which has been shown to increase the fusogenicity and endosomal escape of LNPs[12,43]. In this reaction, we noticed that, compared with aromatic alkynes, aliphatic alkynes are less efficient in synthesizing dipropargylamines but equally efficient in synthesizing monopropargylamines. While the typical yield in our current synthetic scheme is modest in most cases, increased yields are expected when more efficient catalysts are used[44,45].

Our results suggest that asymmetric A^3-lipids tend to show higher in vivo transfection efficacy than symmetric ones (Library 2 vs Libraries 3 and 4), which is supported by others[25,26,46]. Interestingly, several industry ionizable lipids (including SM-102 and LP01) recently chosen for clinical development are asymmetric, in contrast to the symmetric tail structure of the early developed MC3 (ref. 1). We noticed that our lead asymmetric A^3-lipids share some structural features, including an amino-diacid motif, two ionizable nitrogens, two 2° esters and pseudo-three tails. These A^3-lipids exhibit structural similarity to industry ionizable lipids rather than many literature ones, where a polyamine core is typically attached to multiple alkyl tails[7–9]. Our lead 31hP LNP exhibited higher stability and durability compared with MC3 LNP and SM-102 LNP at refrigerator temperature, suggesting its advantages in storage and transport. Moreover, 31hP LNP achieved more efficient hepatic mRNA delivery with a much higher gene editing efficiency than MC3 LNP and LP01 LNP when CRISPR gene editors were delivered. With regard to intramuscular mRNA vaccine delivery, 31hP LNP triggered higher antibody responses than SM-102 LNP following a prime–boost vaccination strategy. Further mechanistic investigation is warranted to understand the strong immunogenicity of 31hP LNP vaccine. Nevertheless, these results suggest that ionizable lipids generated through a directed chemical evolution strategy can rapidly reach, and even surpass, the potency of industry ionizable lipids that were developed over years.

In summary, we established an activity- and biodegradability-driven directed chemical evolution approach for the accelerated structural optimization of A^3-lipids through iterative, rationale-driven mutation and selection. An A^3-coupling reaction was applied and developed to synthesize A^3-lipids with desired properties following five rounds of iteration. Dozens of potent, biodegradable, asymmetric A^3-lipids were identified, and their key structural criteria are reported. The lead A^3-lipid showed superior hepatic delivery of gene editors and intramuscular delivery of mRNA vaccines compared with several industry standard ionizable lipids, highlighting the potential of this ionizable lipid for therapeutic and vaccine applications. We foresee that our

directed-chemical-evolution methodology and resulting structural criteria can accelerate the development of desirable ionizable lipids for a broad range of mRNA delivery applications.

Methods

Materials

Amines, aldehydes, alkynes, alcohols, carboxylic acids, *N*,*N*′-dicyclohexylcarbodiimide (DCC), 4-dimethylaminopyridine (DMAP) and copper(I) chloride were purchased from Sigma Aldrich, Tokyo Chemical Industry, Ambeed and AstaTech. 1,2-dioleoyl-*sn*-glycero-3-phosphoethanolamine (DOPE), 1,2-distearoyl-*sn*-glycero-3-phosphocholine (DSPC), 1,2-dimyristoyl-rac-glycero-3-methoxypolyethylene glycol-2000 (DMG-PEG 2000) and cholesterol were obtained from Avanti Polar Lipids. DLin-MC3-DMA and SM-102 were purchased from MedChem Express. LP01 was purchased from Cayman Chemical. Porcine liver esterase was obtained from Sigma Aldrich. Nucleoside-modified Cas9 mRNA (5moU) was bought from TriLink. Highly modified sgRNA target mouse TTR (guide No. G211) was chemically synthesized by a commercial supplier (AxoLabs) on the basis of a previous publication[40].

mRNA synthesis

Codon-optimized firefly luciferase sequence or SARS-CoV-2 Spike sequence was cloned into a proprietary mRNA production plasmid (optimized 3′ and 5′ UTR with a 101 polyA tail), in vitro transcribed in the presence of 1-methyl pseudouridine modified nucleoside, co-transcriptionally capped using the CleanCap technology (TriLink) and cellulose purified to remove double-stranded RNAs. Purified mRNA was ethanol precipitated, washed, resuspended in nuclease-free water and subjected to quality control. All mRNAs were stored at −20 °C until use.

Synthesis of biodegradable aldehydes and alkynes

Details on the synthesis and characterization of biodegradable aldehydes and alkynes are provided in Supplementary Information.

Combinatorial synthesis of A^3-lipids in Libraries 1 and 2

These A^3-lipids were synthesized via solvent-free, copper(I) chloride catalysed A^3-coupling of amine, formaldehyde and alkyne (Method A)[18]. Excess formaldehyde and alkyne (1.25 eq. of −NH−) were used to ensure repeated A^3-coupling reactions. Taking amine 11 as an example, amine 11 (0.1 mmol, 1 eq.), formaldehyde (0.25 mmol, 37% in water, 2.5 eq.), alkyne (0.25 mmol, 2.5 eq.) and copper(I) chloride (0.01 mmol, 0.1 eq.) were combined in a glass vial and stirred at 50 °C for 48 h. Excess triethylamine was added to the reaction if the amine was in the salt form. The yield was typically ~50% for aromatic alkynes and <10% for aliphatic alkynes. The crude A^3-lipids in Library 1 were dissolved in ethanol and directly used for in vitro screening. The crude A^3-lipids in Library 2 as well as the lead A^3-lipid in Library 1 were purified using a CombiFlash NextGen 300+ chromatography system (Teledyne Isco) with gradient elution from 100% dichloromethane (DCM) to 60% DCM/MeOH/NH_4OH (75:22:3, aqueous), and target products were confirmed by MS and ^1H NMR. The yield was typically ~50%.

Combinatorial synthesis of A^3-lipids in Libraries 3–5

These A^3-lipids were synthesized via A^3-coupling of amine, long-chain aldehyde and long-chain alkyne (Method B). Excess amine (1.25 eq. of aldehyde/alkyne) was used. Taking amine 31 as an example, amine 31 (0.125 mmol, 1.25 eq.), long-chain aldehyde (0.1 mmol, 1 eq.), long-chain alkyne (0.1 mmol, 1 eq.) and copper(I) chloride (0.01 mmol, 0.1 eq.) were combined in a glass vial and stirred at 50 °C for 48 h. The crude products in Libraries 3–5 were purified using a CombiFlash NextGen 300+ chromatography system with gradient elution from 100% DCM to 80% DCM/MeOH/NH_4OH (75:22:3, aqueous), and target products were confirmed by MS and ^1H NMR. The yield was typically ~50%.

LNP formulation

For in vitro and in vivo screening of Libraries 1–5, A^3-LNPs were prepared by pipette mixing of the ethanolic phase containing A^3-lipid, DOPE, cholesterol and DMG-PEG, with the aqueous phase (10 mM citrate buffer, pH 3) containing mLuc at a volume ratio of 1:3. The weight ratio of A^3-lipid:DOPE:cholesterol:DMG-PEG:mRNA was fixed at 16:10:10:3:1.6. The hydrodynamic size of A^3-LNP formulated by pipette mixing was typically 100–200 nm and the mRNA encapsulation efficiency was typically 60–80%.

For therapeutic mRNA delivery, LNPs were formulated by microfluidic mixing. The ethanolic phase containing lipids (A^3-lipid:DOPE:Chol:DMG-PEG = 40:10:48.8:1.5 (ref. 47)) was mixed with the aqueous phase containing mRNA at a flow rate ratio of 1:3 and at an A^3-lipid:mRNA weight ratio of 10:1 in a microfluidic chip device[48]. The standard MC3 LNP (or SM-102 LNP) was formulated with MC3 (or SM-102), DSPC, cholesterol and DMG-PEG at a molar ratio of 50:10:38.5:1.5 using microfluidic mixing at an ionizable lipid:mRNA weight ratio of 10:1. The standard LP01 LNP was formulated according to a previous study[32]. LNPs were dialysed against 1× PBS in a 20 kDa MWCO cassette for 2 h, filtered through a 0.22 μM filter and stored at 4 °C.

Characterization

^1H NMR was recorded using a Bruker 400 MHz NMR spectrometer. MS was performed on a Waters Acquity LC–MS system equipped with UV-Vis and MS detectors. The hydrodynamic size, PDI and zeta potential of LNPs were measured using a Malvern Zetasizer Nano ZS90 instrument. The morphology of LNPs was characterized using a cryo-electron microscope (Titan Krios, Thermo Fisher) equipped with a K3 Bioquantum. The mRNA encapsulation efficiency and the pK_a of LNP were determined using a modified Quant-iT RiboGreen RNA assay (Invitrogen) and a 6-(*p*-toluidinyl)naphthalene-2-sulfonic acid (TNS) assay[49], respectively.

Molecular modelling

Molecular models of 31hP were drawn using DS ViewerPro (v.5.0) software. Material Studio Modelling (v.3.1) software from Accelrys was used to perform the energy minimizations of the built models on the supramolecular structures. BIOVIA Discovery Studio Visualizer (v.2019) was used for display style and colouring.

Cell culture and animal studies

The human hepatocellular carcinoma HepG2 cell line was purchased from American Type Culture Collection (ATCC) and maintained in Dulbecco's modified Eagle medium (DMEM) supplemented with 10% fetal bovine serum (FBS), 100 U ml^{-1} penicillin and 100 μg ml^{-1} streptomycin. Cells were cultured at 37 °C in a humidified incubator with 5% CO_2 and routinely tested for mycoplasma contamination.

All animal protocols were approved by the Institutional Animal Care and Use Committee of the University of Pennsylvania (806540), and animal procedures were performed in accordance with the Guidelines for the Care and Use of Laboratory Animals at the University of Pennsylvania. C57BL/6 female mice (6–8 weeks, 18–20 g) were purchased from Jackson Laboratory and housed in a specific-pathogen-free animal facility at ambient temperature (22 ± 2 °C), air humidity (40%–70%) and 12-h dark/12-h light cycle.

In vitro mLuc delivery by A^3-LNPs

HepG2 cells were seeded in 96-well plates at a density of 5,000 per well overnight and mLuc-loaded A^3-LNPs (15 ng mRNA per well) were used to treat cells for 24 h. Luciferase expression was evaluated using the Luciferase Reporter 1000 Assay system (Promega, E4550) and cell viability was measured using a CellTiter-Glo Luminescent Cell Viability Assay system (Promega, G7572) according to manufacturer protocols.

In vivo mLuc delivery by A^3-LNPs

Mice were i.v. injected with mLuc-loaded A^3-LNPs at an mRNA dose of 0.1 mg kg−1. For i.m. delivery, mLuc-loaded A^3-LNPs (2 μg mRNA in 50 μl PBS) were injected into the gastrocnemius muscle. After 4 h, mice were intraperitoneally (i.p.) injected with D-luciferin potassium salt (150 mg kg^{-1}), and bioluminescence imaging was performed using an in vivo imaging system (PerkinElmer).

Haemolysis assay

Mouse red blood cells (RBCs) were isolated and washed three times with 1× PBS by centrifugation at 700 *g* for 5 min. Next, RBCs were diluted to a 4% v/v RBC solution either in neutral (pH 7.4) or acidic (pH 6.0) PBS, and incubated with LNPs at a final mRNA concentration of 3 μg ml^{-1} at 37 °C for 1 h. Finally, the RBC solution was centrifuged at 700 *g* for 5 min and 100 μl supernatant was transferred into a 96-well plate. The absorption at 540 nm was determined with a plate reader. Positive and negative controls were carried out with 0.1% Triton-X and 1× PBS, respectively.

Cellular internalization inhibition

HepG2 cells were seeded in a 96-well plate at a density of 5,000 per well overnight. Cells were pretreated with 5 mM amiloride, 20 μM chlorpromazine, 0.2 mM genistein or 5 mM Mβ-CD for 30 min. A control group was pretreated with dimethylsulfoxide (DMSO). Then, cells were treated with mLuc-loaded LNPs (15 ng per well) for 24 h. Luciferase expression was determined as described above and normalized to the control.

Biodegradability analysis

Ionizable lipid at 0.5 mg ml^{-1} in 1× PBS was incubated with or without porcine liver esterase (100 U ml^{-1}) at 37 °C for 12 h. The incubation solution was mixed with a 10-fold volume of acetonitrile to terminate the reaction, and the mixture was centrifuged at 10,000 r.p.m. for 5 min. The remaining ionizable lipid in the supernatant was analysed using LC–MS.

Systemic delivery of CRISPR gene editor

Mice were i.v. injected with Cas9 mRNA/TTR sgRNA (4:1, w/w)-loaded LNPs at a total RNA dose of 1 mg kg^{-1}. Serum was collected on day 7 and analysed by enzyme-linked immunosorbent assay (ELISA) (Aviva Systems Biology, OKIA00111). Mice were euthanized and livers were collected to determine the on-target indel frequency by next-generation sequencing (NGS). For TTR on-target DNA sequencing, DNA was extracted from the liver using the Qiagen Puregene Tissue kit (158063) and quantified using a Nanodrop 2000 spectrophotometer. PCR amplification of the TTR target site was carried out using Q5 High-Fidelity DNA polymerase (New England Biolabs, M0491) and the following primer sequences: mTTR-exon2-F, 5′-CGGTTTACTCTGACCCATTTC-3′ and mTTR-exon2-R, 5′-GGGCTTTCTACAAGCTTACC-3′. Deep sequencing of the TTR amplicons and determination of the on-target indel frequency were performed essentially as described except that 150 bp paired-end reads were produced[50].

Intramuscular delivery of SARS-CoV-2 mRNA vaccine

Mice were i.m. injected with SARS-CoV-2 Spike mRNA-loaded LNPs (2 μg mRNA in 50 μl PBS) twice using a prime–boost strategy at a 3-week interval. Serum was acquired at 5 weeks post prime vaccination. Anti-Spike IgG titres and pseudovirus neutralization antibody titres against D614G-mutated SARS-CoV-2 ancestor strain were determined.

To determine anti-Spike IgG titres, 96-well clear polystyrene high bind Stripwell microplates (Corning) were coated overnight with 1 μg ml^{-1} purified SARS-CoV-2 His-tagged Spike protein (Sino Biological, 40589-V08H8). Plates were washed once with wash buffer (0.05% Tween-20 in PBS) and blocked for 2 h at room temperature using a solution of heat-inactivated, IgG-depleted, protease-free bovine serum albumin (2% w/v BSA in PBS). After blocking, plates were washed three times and mouse serum was serially diluted in the blocking solution and incubated for 2 h at r.t. Plates were washed three times before the addition of HRP-conjugated anti-mouse secondary antibody specific to IgG (1:10,000, Abcam, ab97040) in blocking buffer. Plates were incubated for 1.5 h and washed three times before the addition of 100 μl per well of KPL TMB substrate for 8 min. The reaction was stopped by adding 50 μl of 2 N sulfuric acid and the absorbance was measured at 450 nm using a SpectraMax 190 microplate reader. Spike-specific IgG end-point dilution titre was defined as the highest dilution of serum to give an optical density (OD) greater than the cut-off OD value determined using the Frey method[34,51].

Pseudovirus neutralization assay was performed using a lentivirus-based system expressing the D614G Spike protein (Integral Molecular, RVP-702L). HEK-293/ACE-II cells were seeded at a density of 20,000 cells per well in 96-well plates overnight. Serum samples were serially diluted in RPMI-1640 medium and incubated with an equivalent volume (1:1, v/v) of lentivirus-based pseudovirus expressing *Renilla* luciferase (50 foci forming units). The lentivirus–serum mixture was incubated at 37 °C for 1 h to allow interaction between neutralizing antibodies and pseudovirus particles. The mixture (100 μl) was then added to HEK-293/ACE-II cells and incubated for 48 h. Luciferase expression was evaluated using the *Renilla*-Glo Luciferase Assay system (Promega, E2710) according to manufacturer protocols. The 50% neutralization titre (NT_{50}) was determined as the greatest serum dilution at which the luminescence was reduced by 50% relative to control cells treated with the pseudovirus in the absence of serum. NT_{50} titres for each sample were measured in two technical replicates performed on separate days.

Safety evaluation

Serum was collected at 24 h post treatment of Cas9 mRNA/TTR sgRNA-loaded LNPs (1 mg kg^{-1}) or 31hP-M (a degradation metabolite of 31hP, 5 mg kg^{-1}). ALT and AST activities were determined using the alanine transaminase colorimetric activity assay kit (700260, Cayman) and aspartate aminotransferase colorimetric activity assay kit (701640, Cayman), respectively. Thirteen pro-inflammatory cytokines were examined using a LEGENDplex multi-analyte flow assay kit (BioLegend, 740621) according to manufacturer instruction.

Statistical analysis

Data are presented as mean ± s.d. Student's *t*-test or one-way analysis of variance (ANOVA) followed by Tukey's test was applied for comparison between two groups or among multiple groups, respectively, using Graphpad Prism 8.0. $P < 0.05$ was considered statistically significant.

Reporting summary

Further information on research design is available in the Nature Portfolio Reporting Summary linked to this article.

Data availability

All relevant data supporting the findings of this study are available within the paper and its Supplementary Information. Source data are provided with this paper.

References

1. Han, X. et al. An ionizable lipid toolbox for RNA delivery. *Nat. Commun.* **12**, 7233 (2021).
2. Hou, X., Zaks, T., Langer, R. & Dong, Y. Lipid nanoparticles for mRNA delivery. *Nat. Rev. Mater.* **6**, 1078–1094 (2021).
3. Eygeris, Y., Gupta, M., Kim, J. & Sahay, G. Chemistry of lipid nanoparticles for RNA delivery. *Acc. Chem. Res.* **55**, 2–12 (2022).
4. Zhang, Y., Sun, C., Wang, C., Jankovic, K. E. & Dong, Y. Lipids and lipid derivatives for RNA delivery. *Chem. Rev.* **121**, 12181–12277 (2021).
5. Semple, S. C. et al. Rational design of cationic lipids for siRNA delivery. *Nat. Biotechnol.* **28**, 172–176 (2010).

6. Jayaraman, M. et al. Maximizing the potency of siRNA lipid nanoparticles for hepatic gene silencing in vivo. *Angew. Chem. Int. Ed. Engl.* **51**, 8529–8533 (2012).
7. Akinc, A. et al. A combinatorial library of lipid-like materials for delivery of RNAi therapeutics. *Nat. Biotechnol.* **26**, 561–569 (2008).
8. Love, K. T. et al. Lipid-like materials for low-dose, in vivo gene silencing. *Proc. Natl. Acad. Sci. USA* **107**, 1864–1869 (2010).
9. Whitehead, K. A. et al. Degradable lipid nanoparticles with predictable in vivo siRNA delivery activity. *Nat. Commun.* **5**, 4277 (2014).
10. Miao, L. et al. Delivery of mRNA vaccines with heterocyclic lipids increases anti-tumor efficacy by STING-mediated immune cell activation. *Nat. Biotechnol.* **37**, 1174–1185 (2019).
11. Altinoglu, S., Wang, M. & Xu, Q. Combinatorial library strategies for synthesis of cationic lipid-like nanoparticles and their potential medical applications. *Nanomedicine* **10**, 643–657 (2015).
12. Li, B. et al. Combinatorial design of nanoparticles for pulmonary mRNA delivery and genome editing. *Nat. Biotechnol.* **41**, 1410–1415 (2023).
13. Rhym, L. H., Manan, R. S., Koller, A., Stephanie, G. & Anderson, D. G. Peptide-encoding mRNA barcodes for the high-throughput in vivo screening of libraries of lipid nanoparticles for mRNA delivery. *Nat. Biomed. Eng.* **7**, 901–910 (2023).
14. Packer, M. S. & Liu, D. R. Methods for the directed evolution of proteins. *Nat. Rev. Genet.* **16**, 379–394 (2015).
15. Wang, Y. et al. Directed evolution: methodologies and applications. *Chem. Rev.* **121**, 12384–12444 (2021).
16. Esvelt, K. M., Carlson, J. C. & Liu, D. R. A system for the continuous directed evolution of biomolecules. *Nature* **472**, 499–503 (2011).
17. Peshkov, V. A., Pereshivko, O. P. & Van der Eycken, E. V. A walk around the A^3-coupling. *Chem. Soc. Rev.* **41**, 3790–3807 (2012).
18. Uhlig, N. & Li, C. J. Site-specific modification of amino acids and peptides by aldehyde-alkyne-amine coupling under ambient aqueous conditions. *Org. Lett.* **14**, 3000–3003 (2012).
19. Jesin, I. & Nandi, G. C. Recent advances in the A^3 coupling reactions and their applications. *Eur. J. Org. Chem.* **2019**, 2704–2720 (2019).
20. Bonfield, E. R. & Li, C. J. Efficient ruthenium and copper cocatalyzed five-component coupling to form dipropargyl amines under mild conditions in water. *Org. Biomol. Chem.* **5**, 435–437 (2007).
21. Hajj, K. A. et al. Branched-tail lipid nanoparticles potently deliver mRNA in vivo due to enhanced ionization at endosomal pH. *Small* **15**, e1805097 (2019).
22. Zhang, X. et al. Functionalized lipid-like nanoparticles for in vivo mRNA delivery and base editing. *Sci. Adv.* **6**, eabc2315 (2020).
23. Hashiba, K. et al. Branching ionizable lipids can enhance the stability, fusogenicity, and functional delivery of mRNA. *Small Sci.* **3**, 2200071 (2023).
24. Paunovska, K. et al. A direct comparison of in vitro and in vivo nucleic acid delivery mediated by hundreds of nanoparticles reveals a weak correlation. *Nano Lett.* **18**, 2148–2157 (2018).
25. Lu, J. et al. Screening libraries to discover molecular design principles for the targeted delivery of mRNA with one-component ionizable amphiphilic janus dendrimers derived from plant phenolic acids. *Pharmaceutics* **15**, eabc2315 (2023).
26. Sabnis, S. et al. A novel amino lipid series for mRNA delivery: improved endosomal escape and sustained pharmacology and safety in non-human primates. *Mol. Ther.* **26**, 1509–1519 (2018).
27. Holthuis, J. C. & Menon, A. K. Lipid landscapes and pipelines in membrane homeostasis. *Nature* **510**, 48–57 (2014).
28. Zhang, D. et al. One-component multifunctional sequence-defined ionizable amphiphilic janus dendrimer delivery systems for mRNA. *J. Am. Chem. Soc.* **143**, 12315–12327 (2021).
29. Lam, K. et al. Unsaturated, trialkyl ionizable lipids are versatile lipid-nanoparticle components for therapeutic and vaccine applications. *Adv. Mater.* **35**, e2209624 (2023).
30. Maier, M. A. et al. Biodegradable lipids enabling rapidly eliminated lipid nanoparticles for systemic delivery of RNAi therapeutics. *Mol. Ther.* **21**, 1570–1578 (2013).
31. Li, L., Hu, S. & Chen, X. Non-viral delivery systems for CRISPR/Cas9-based genome editing: challenges and opportunities. *Biomaterials* **171**, 207–218 (2018).
32. Finn, J. D. et al. A single administration of CRISPR/Cas9 lipid nanoparticles achieves robust and persistent in vivo genome editing. *Cell Rep.* **22**, 2227–2235 (2018).
33. Alameh, M. G. et al. Lipid nanoparticles enhance the efficacy of mRNA and protein subunit vaccines by inducing robust T follicular helper cell and humoral responses. *Immunity* **54**, 2877–2892.e7 (2021).
34. Han, X. et al. Adjuvant lipidoid-substituted lipid nanoparticles augment the immunogenicity of SARS-CoV-2 mRNA vaccines. *Nat. Nanotechnol.* **18**, 1105–1114 (2023).
35. Chen, J. et al. Lipid nanoparticle-mediated lymph node-targeting delivery of mRNA cancer vaccine elicits robust $CD8^+$ T cell response. *Proc. Natl Acad. Sci. USA* **119**, e2207841119 (2022).
36. Semple, S. C. et al. Efficient encapsulation of antisense oligonucleotides in lipid vesicles using ionizable aminolipids: formation of novel small multilamellar vesicle structures. *Biochim. Biophys. Acta Biomembranes* **1510**, 152–166 (2001).
37. Hassett, K. J. et al. Optimization of lipid nanoparticles for intramuscular administration of mRNA vaccines. *Mol. Ther. Nucleic acids* **15**, 1–11 (2019).
38. Cornebise, M. et al. Discovery of a novel amino lipid that improves lipid nanoparticle performance through specific interactions with mRNA. *Adv. Funct. Mater.* **32**, 2106727 (2022).
39. Maheshri, N., Koerber, J. T., Kaspar, B. K. & Schaffer, D. V. Directed evolution of adeno-associated virus yields enhanced gene delivery vectors. *Nat. Biotechnol.* **24**, 198–204 (2006).
40. Tabebordbar, M. et al. Directed evolution of a family of AAV capsid variants enabling potent muscle-directed gene delivery across species. *Cell* **184**, 4919–4938.e22 (2021).
41. Rajappan, K. et al. Property-driven design and development of lipids for efficient delivery of siRNA. *J. Med. Chem.* **63**, 12992–13012 (2020).
42. Xu, Y. et al. AGILE platform: a deep learning-powered approach to accelerate LNP development for mRNA delivery. *Nat. Commun.* **15**, 6305 (2024).
43. Miao, L. et al. Synergistic lipid compositions for albumin receptor mediated delivery of mRNA to the liver. *Nat. Commun.* **11**, 2424 (2020).
44. Wei, C., Li, Z. & Li, C.-J. The development of A^3-coupling (aldehyde-alkyne-amine) and AA^3-coupling (asymmetric aldehyde-alkyne-amine). *Synlett* **2004**, 1472–1483 (2004).
45. Rokade, B. V., Barker, J. & Guiry, P. J. Development of and recent advances in asymmetric A^3 coupling. *Chem. Soc. Rev.* **48**, 4766–4790 (2019).
46. Suzuki, Y. et al. Design and lyophilization of lipid nanoparticles for mRNA vaccine and its robust immune response in mice and nonhuman primates. *Mol. Ther. Nucleic acids* **30**, 226–240 (2022).
47. Zhang, R. et al. Helper lipid structure influences protein adsorption and delivery of lipid nanoparticles to spleen and liver. *Biomater. Sci.* **9**, 1449–1463 (2021).
48. Han, X. et al. Ligand-tethered lipid nanoparticles for targeted RNA delivery to treat liver fibrosis. *Nat. Commun.* **14**, 75 (2023).
49. Billingsley, M. M. et al. Ionizable lipid nanoparticle-mediated mRNA delivery for human CAR T cell engineering. *Nano Lett.* **20**, 1578–1589 (2020).

50. Wang, L. et al. Meganuclease targeting of PCSK9 in macaque liver leads to stable reduction in serum cholesterol. *Nat. Biotechnol.* **36**, 717–725 (2018).
51. Frey, A., Di Canzio, J. & Zurakowski, D. A statistically defined endpoint titer determination method for immunoassays. *J. Immunol. Methods* **221**, 35–41 (1998).

Acknowledgements

M.J.M. acknowledges support from a US National Institutes of Health (NIH) Director's New Innovator Award (DP2 TR002776), a Burroughs Wellcome Fund Career Award at the Scientific Interface (CASI) and an American Cancer Society Research Scholar Grant (RSG-22-122-01-ET). J.M.W. acknowledges support from iECURE. We thank S. Steimle from the Beckman Center for Cryo Electron Microscopy at UPenn Perelman School of Medicine (RRID: SCR_022375) for help in characterizing the morphology of LNPs; the UPenn Gene Therapy Program NAT Core for sequencing service and K. Martins for processing the NGS data.

Author contributions

X.H. and M.J.M. conceptualized the project. X.H. and M.-G.A. developed the methodology. X.H., M.-G.A., Y.X., R.P., J.X., R.E.-M., G.D., C.C.W. and I.-C.Y. conducted investigations. X.H. and Y.X. performed visualization. M.J.M. acquired funding and supervised the project. X.H. and M.J.M. wrote the original draft. J.X., M.-G.A., Y.X., R.P., L.X., N.G., R.E.-M., K.L.S., Q.S., C.C.W., J.M.W., D.W. and M.J.M. reviewed and edited the manuscript.

Competing interests

X.H. and M.J.M. have filed a patent application based on this work. J.M.W. is a paid advisor to and holds equity in iECURE, Passage Bio, and the Center for Breakthrough Medicines (CBM). He also holds equity in the former G2 Bio asset companies and Ceva Santé Animale. He has sponsored research agreements with Alexion Pharmaceuticals, Amicus Therapeutics, CBM, Ceva Santé Animale, Elaaj Bio, FA212, Foundation for Angelman Syndrome Therapeutics, former G2 Bio asset companies, iECURE, and Passage Bio, which are licensees of Penn technology. J.M.W. and C.C.W. are inventors on patents that have been licensed to various biopharmaceutical companies and for which they may receive payments. The other authors declare no competing interests.

Additional information

Supplementary information The online version contains supplementary material available at https://doi.org/10.1038/s41551-024-01267-7.

Correspondence and requests for materials should be addressed to Michael J. Mitchell.

Peer review information *Nature Biomedical Engineering* thanks Hideyoshi Harashima and the other, anonymous, reviewer(s) for their contribution to the peer review of this work.

Reprints and permissions information is available at www.nature.com/reprints.

Publisher's note Springer Nature remains neutral with regard to jurisdictional claims in published maps and institutional affiliations.

[1]Department of Bioengineering, University of Pennsylvania, Philadelphia, PA, USA. [2]Key Laboratory of RNA Innovation, Science and Engineering, CAS Center for Excellence in Molecular Cell Science, Shanghai Institute of Biochemistry and Cell Biology, Chinese Academy of Sciences, University of Chinese Academy of Sciences, Shanghai, China. [3]Department of Medicine, University of Pennsylvania, Philadelphia, PA, USA. [4]Penn Institute for RNA Innovation, Perelman School of Medicine, University of Pennsylvania, Philadelphia, PA, USA. [5]Gene Therapy Program, Perelman School of Medicine, University of Pennsylvania, Philadelphia, PA, USA. [6]Abramson Cancer Center, Perelman School of Medicine, University of Pennsylvania, Philadelphia, PA, USA. [7]Institute for Immunology, Perelman School of Medicine, University of Pennsylvania, Philadelphia, PA, USA. [8]Cardiovascular Institute, Perelman School of Medicine, University of Pennsylvania, Philadelphia, PA, USA. [9]Institute for Regenerative Medicine, Perelman School of Medicine, University of Pennsylvania, Philadelphia, PA, USA. ✉e-mail: mjmitch@seas.upenn.edu

nature portfolio

Corresponding author(s): Michael J. Mitchell

Last updated by author(s): Aug 10, 2024

Reporting Summary

Nature Portfolio wishes to improve the reproducibility of the work that we publish. This form provides structure for consistency and transparency in reporting. For further information on Nature Portfolio policies, see our Editorial Policies and the Editorial Policy Checklist.

Statistics

For all statistical analyses, confirm that the following items are present in the figure legend, table legend, main text, or Methods section.

n/a	Confirmed
☐	☒ The exact sample size (*n*) for each experimental group/condition, given as a discrete number and unit of measurement
☐	☒ A statement on whether measurements were taken from distinct samples or whether the same sample was measured repeatedly
☐	☒ The statistical test(s) used AND whether they are one- or two-sided *Only common tests should be described solely by name; describe more complex techniques in the Methods section.*
☒	☐ A description of all covariates tested
☐	☒ A description of any assumptions or corrections, such as tests of normality and adjustment for multiple comparisons
☐	☒ A full description of the statistical parameters including central tendency (e.g. means) or other basic estimates (e.g. regression coefficient) AND variation (e.g. standard deviation) or associated estimates of uncertainty (e.g. confidence intervals)
☐	☒ For null hypothesis testing, the test statistic (e.g. *F*, *t*, *r*) with confidence intervals, effect sizes, degrees of freedom and *P* value noted *Give P values as exact values whenever suitable.*
☒	☐ For Bayesian analysis, information on the choice of priors and Markov chain Monte Carlo settings
☒	☐ For hierarchical and complex designs, identification of the appropriate level for tests and full reporting of outcomes
☒	☐ Estimates of effect sizes (e.g. Cohen's *d*, Pearson's *r*), indicating how they were calculated

Our web collection on statistics for biologists contains articles on many of the points above.

Software and code

Policy information about availability of computer code

Data collection	Bruker 400 MHz NMR spectrometer, Zetasizer Nano ZS90, IVIS spectrum.
Data analysis	Statistical analysis was performed on Graphpad Prism 8.0, 1H NMR spectrum was analysed by MestReNova x64, in vivo imaging analysis (total flux) was performed on IVIS spectrum, and molecular simulation was performed on BIOVIA Discovery Studio 2018.

For manuscripts utilizing custom algorithms or software that are central to the research but not yet described in published literature, software must be made available to editors and reviewers. We strongly encourage code deposition in a community repository (e.g. GitHub). See the Nature Portfolio guidelines for submitting code & software for further information.

Data

Policy information about availability of data

All manuscripts must include a data availability statement. This statement should provide the following information, where applicable:

- Accession codes, unique identifiers, or web links for publicly available datasets
- A description of any restrictions on data availability
- For clinical datasets or third party data, please ensure that the statement adheres to our policy

All relevant data supporting the findings of this study are available within the paper and the Supplementary Information. Source data are provided with this paper.

Research involving human participants, their data, or biological material

Policy information about studies with human participants or human data. See also policy information about sex, gender (identity/presentation), and sexual orientation and race, ethnicity and racism.

Reporting on sex and gender	The study did not involve human research participants.
Reporting on race, ethnicity, or other socially relevant groupings	–
Population characteristics	–
Recruitment	–
Ethics oversight	–

Note that full information on the approval of the study protocol must also be provided in the manuscript.

Field-specific reporting

Please select the one below that is the best fit for your research. If you are not sure, read the appropriate sections before making your selection.

☒ Life sciences ☐ Behavioural & social sciences ☐ Ecological, evolutionary & environmental sciences

For a reference copy of the document with all sections, see nature.com/documents/nr-reporting-summary-flat.pdf

Life sciences study design

All studies must disclose on these points even when the disclosure is negative.

Sample size	No statistical methods were used to determine sample sizes. Sample sizes were determined by allowable error size, accuracy, resources, and need for statistical analysis (generally n>=3 throughout all the studies). For initial screening, n=2 was used for rapid and cost-efficient screening of lipid candidates.
Data exclusions	No animals and/or data were excluded.
Replication	All experiments were repeated for at least three times, and the experimental findings were reproducible.
Randomization	For the in vivo study, animal groups were randomized by body weight. For other experiments, all samples were randomly allocated into experimental groups, as there was no covariate in the study design.
Blinding	All the investigators were blinded to group allocation during data collection and analysis.

Reporting for specific materials, systems and methods

We require information from authors about some types of materials, experimental systems and methods used in many studies. Here, indicate whether each material, system or method listed is relevant to your study. If you are not sure if a list item applies to your research, read the appropriate section before selecting a response.

Materials & experimental systems

n/a	Involved in the study
☐	☒ Antibodies
☐	☒ Eukaryotic cell lines
☒	☐ Palaeontology and archaeology
☐	☒ Animals and other organisms
☒	☐ Clinical data
☒	☐ Dual use research of concern
☒	☐ Plants

Methods

n/a	Involved in the study
☒	☐ ChIP-seq
☒	☐ Flow cytometry
☒	☐ MRI-based neuroimaging

Antibodies

Antibodies used	HRP-conjugated anti-mouse secondary antibody specific to IgG (1:10,000, Abcam, #ab97040).

Validation	All antibodies were verified by the supplier, and each lot had been quality-tested. All the antibodies used are from commercial sources, and had been validated by the vendors. Validation data are available on the manufacturer's website.

Eukaryotic cell lines

Policy information about cell lines and Sex and Gender in Research

Cell line source(s)	HepG2 cells were obtained from American Type Culture Collection (ATCC, #HB-8065).
Authentication	A short tandem repeat DNA-profiling method was used to authenticate the cell lines, and the results were compared with reference databases.
Mycoplasma contamination	The cells were tested for mycoplasma contamination. No mycoplasma contamination was found.
Commonly misidentified lines (See ICLAC register)	No commonly misidentified cell lines were used.

Animals and other research organisms

Policy information about studies involving animals; ARRIVE guidelines recommended for reporting animal research, and Sex and Gender in Research

Laboratory animals	C57BL/6 female mice (6–8 weeks, 18–20 g) were purchased from The Jackson Laboratory, and housed in a specific-pathogen-free animal facility at ambient temperature (22 ± 2 °C), air humidity 40%–70% and a 12-h dark/12-h light cycle.
Wild animals	The study did not involve wild animals.
Reporting on sex	Female mice were used. Sex should not affect the results.
Field-collected samples	The study did not involve samples collected from field.
Ethics oversight	All animal protocols were approved by the Institutional Animal Care and Use Committee (IACUC) of University of Pennsylvania (#806540), and animal procedures were performed in accordance with the Guidelines for Care and Use of Laboratory Animals at the University of Pennsylvania.

Note that full information on the approval of the study protocol must also be provided in the manuscript.